

# World Journal of *Radiology*

*World J Radiol* 2018 April 28; 10(4): 30-45





**REVIEW**

- 30**    Susceptibility weighted imaging: Clinical applications and future directions

*Halefoglu AM, Yousem DM*

**ABOUT COVER**

Editorial Board Member of *World Journal of Radiology*, Edward Araujo Júnior, PhD, Associate Professor, Department of Obstetrics, Paulista School of Medicine - Federal University of Sao Paulo, São Paulo 05089-030, Brazil

**AIM AND SCOPE**

*World Journal of Radiology* (*World J Radiol*, *WJR*, online ISSN 1949-8470, DOI: 10.4329) is a peer-reviewed open access academic journal that aims to guide clinical practice and improve diagnostic and therapeutic skills of clinicians.

*WJR* covers topics concerning diagnostic radiology, radiation oncology, radiologic physics, neuroradiology, nuclear radiology, pediatric radiology, vascular/interventional radiology, medical imaging achieved by various modalities and related methods analysis. The current columns of *WJR* include editorial, frontier, diagnostic advances, therapeutics advances, field of vision, mini-reviews, review, topic highlight, medical ethics, original articles, case report, clinical case conference (clinicopathological conference), and autobiography.

We encourage authors to submit their manuscripts to *WJR*. We will give priority to manuscripts that are supported by major national and international foundations and those that are of great basic and clinical significance.

**INDEXING/ABSTRACTING**

*World Journal of Radiology* is now indexed in PubMed, PubMed Central, and Emerging Sources Citation Index (Web of Science).

**EDITORS FOR THIS ISSUE**

Responsible Assistant Editor: *Xiang Li*  
Responsible Electronic Editor: *Wen-Wen Tan*  
Proofing Editor-in-Chief: *Lian-Sheng Ma*

Responsible Science Editor: *Fang-Fang Ji*  
Proofing Editorial Office Director: *Jin-Lei Wang*

**NAME OF JOURNAL**  
*World Journal of Radiology*

**ISSN**  
ISSN 1949-8470 (online)

**LAUNCH DATE**  
January 31, 2009

**FREQUENCY**  
Monthly

**EDITORS-IN-CHIEF**  
**Kai U Juergens, MD, Associate Professor**, MRT und PET/CT, Nuklearmedizin Bremen Mitte, ZEMODI - Zentrum für morphologische und molekulare Diagnostik, Bremen 28177, Germany

**Edwin JR van Beek, MD, PhD, Professor**, Clinical Research Imaging Centre and Department of Medical Radiology, University of Edinburgh, Edinburgh EH16 4TJ, United Kingdom

**Thomas J Vogl, MD, Professor, Reader in Health Technology Assessment**, Department of Diagnostic and Interventional Radiology, Johann Wolfgang Goethe University of Frankfurt, Frankfurt 60590,

Germany

**EDITORIAL BOARD MEMBERS**  
All editorial board members resources online at <http://www.wjgnet.com/1949-8470/editorialboard.htm>

**EDITORIAL OFFICE**  
Jin-Lei Wang, Director  
*World Journal of Radiology*  
Baishideng Publishing Group Inc  
7901 Stoneridge Drive, Suite 501, Pleasanton, CA 94588, USA  
Telephone: +1-925-2238242  
Fax: +1-925-2238243  
E-mail: [editorialoffice@wjgnet.com](mailto:editorialoffice@wjgnet.com)  
Help Desk: <http://www.f6publishing.com/helpdesk>  
<http://www.wjgnet.com>

**PUBLISHER**  
Baishideng Publishing Group Inc  
7901 Stoneridge Drive, Suite 501, Pleasanton, CA 94588, USA  
Telephone: +1-925-2238242  
Fax: +1-925-2238243  
E-mail: [bpgoffice@wjgnet.com](mailto:bpgoffice@wjgnet.com)  
Help Desk: <http://www.f6publishing.com/helpdesk>  
<http://www.wjgnet.com>

**PUBLICATION DATE**  
April 28, 2018

**COPYRIGHT**  
© 2018 Baishideng Publishing Group Inc. Articles published by this Open-Access journal are distributed under the terms of the Creative Commons Attribution Non-commercial License, which permits use, distribution, and reproduction in any medium, provided the original work is properly cited, the use is non commercial and is otherwise in compliance with the license.

**SPECIAL STATEMENT**  
All articles published in journals owned by the Baishideng Publishing Group (BPG) represent the views and opinions of their authors, and not the views, opinions or policies of the BPG, except where otherwise explicitly indicated.

**INSTRUCTIONS TO AUTHORS**  
<http://www.wjgnet.com/bpg/gerinfo/204>

**ONLINE SUBMISSION**  
<http://www.f6publishing.com>

## Susceptibility weighted imaging: Clinical applications and future directions

Ahmet Mesrur Halefoglu, David Mark Yousem

Ahmet Mesrur Halefoglu, Department of Radiology, Sisli Hamidiye Etfal Training and Research Hospital, University of Health Sciences, Istanbul 34371, Turkey

David Mark Yousem, Division of Neuroradiology, Department of Radiology, Johns Hopkins Medical Institution, Baltimore, MI 21287, United States

ORCID number: Ahmet Mesrur Halefoglu (0000-0002-2054-3550); David Mark Yousem (0000-0002-1222-6643).

**Author contributions:** All authors equally contributed to this paper with conception and design of the study, literature review and analysis, drafting, critical revision and editing, and final approval of the final version.

**Conflict-of-interest statement:** No potential conflicts of interest.

**Open-Access:** This article is an open-access article which was selected by an in-house editor and fully peer-reviewed by external reviewers. It is distributed in accordance with the Creative Commons Attribution Non Commercial (CC BY-NC 4.0) license, which permits others to distribute, remix, adapt, build upon this work non-commercially, and license their derivative works on different terms, provided the original work is properly cited and the use is non-commercial. See: <http://creativecommons.org/licenses/by-nc/4.0/>

**Manuscript source:** Unsolicited manuscript

**Correspondence to:** Ahmet Mesrur Halefoglu, MD, Professor, Department of Radiology, Sisli Hamidiye Etfal Training and Research Hospital, University of Health Sciences, Birlik sok, Parksaray ap, No: 17/4, Istanbul 34371, Turkey. [halefoglu@hotmail.com](mailto:halefoglu@hotmail.com)  
Telephone: +90-212-3735000  
Fax: +90-212-2415015

Received: March 17, 2018

Peer-review started: March 17, 2018

First decision: April 4, 2018

Revised: April 8, 2018

Accepted: April 20, 2018

Article in press: April 20, 2018

Published online: April 28, 2018

### Abstract

Susceptibility weighted imaging (SWI) is a recently developed magnetic resonance imaging (MRI) technique that is increasingly being used to narrow the differential diagnosis of many neurologic disorders. It exploits the magnetic susceptibility differences of various compounds including deoxygenated blood, blood products, iron and calcium, thus enabling a new source of contrast in MR. In this review, we illustrate its basic clinical applications in neuroimaging. SWI is based on a fully velocity-compensated, high-resolution, three dimensional gradient-echo sequence using magnitude and phase images either separately or in combination with each other, in order to characterize brain tissue. SWI is particularly useful in the setting of trauma and acute neurologic presentations suggestive of stroke, but can also characterize occult low-flow vascular malformations, cerebral microbleeds, intracranial calcifications, neurodegenerative diseases and brain tumors. Furthermore, advanced MRI post-processing technique with quantitative susceptibility mapping, enables detailed anatomical differentiation based on quantification of brain iron from SWI raw data.

**Key words:** Quantitative susceptibility mapping; Brain; Ischemia; Magnetic resonance imaging; Susceptibility weighted imaging

© **The Author(s) 2018.** Published by Baishideng Publishing Group Inc. All rights reserved.

**Core tip:** Susceptibility weighted imaging has a variety of applications in neuroradiology practice and should be included in routine protocols. It can detect micro- and macrohemorrhages and delineate cerebral microvasculature and can also reveal low-flow vascular malformations. It has been proven as a complementary, valuable imaging sequence in the management of stroke patients. It provides differentiation of calcium from hemorrhage in the brain. It plays an important role in the evaluation of traumatic brain injury patients and aids in the characterization and grading of cerebral tumors.



Quantitative susceptibility mapping can be applied on many neurodegenerative disorders by assessing brain iron content.

Halefoglu AM, Yousem DM. Susceptibility weighted imaging: Clinical applications and future directions. *World J Radiol* 2018; 10(4): 30-45 Available from: URL: <http://www.wjgnet.com/1949-8470/full/v10/i4/30.htm> DOI: <http://dx.doi.org/10.4329/wjrv10.i4.30>

## INTRODUCTION

Susceptibility weighted imaging (SWI) is an magnetic resonance imaging (MRI) technique that exploits the magnetic susceptibility differences of various compounds, such as blood, iron, and diamagnetic calcium, thus enabling new sources of MR contrast<sup>[1-3]</sup>.

SWI has been shown to provide clinically useful complementary information to conventional spin-echo MRI sequences. Additionally, through post-processed quantitative susceptibility mapping (QSM) SWI sequences allow data driven research to evaluate compounds that alter the magnetic field of the brain, a strategy most useful in neurodegenerative disorders. In this review, we highlight many clinical applications of SWI in the evaluation and differential diagnosis of diverse central nervous system (CNS) pathologic conditions. We close with an assessment of the future of SWI and QSM.

## PRINCIPLES AND TECHNICAL ASPECTS OF SWI

Local magnetic field heterogeneity leading to T2 shortening may be induced by paramagnetic, diamagnetic and ferromagnetic substances and results in signal loss on T2\* weighted gradient-echo (GE) sequences (proton relaxation enhancement). The susceptibility effect is most visible in non-refocused GE techniques using long echo times (TE), short flip angles, and high field strengths. Although SWI relies on GE sequences, it has enhanced susceptibility sensitivity compared with conventional T2\* weighted GE sequences because it is based on a high-resolution, long TE, flow-compensated, 3D GE imaging technique containing filtered phase information in each voxel<sup>[4]</sup>. In SWI, the magnitude and phase MR data are brought together and a phase mask is created. Multiplying these with the original magnitude images result in a final magnitude SWI dataset. Both magnitude and phase information are essential for proper tissue characterization, and are brought together to create an SWI image<sup>[5]</sup>. Finally, these images are further processed with a minimum intensity projection algorithm (minIP) to obtain 3-10 mm thick high signal to noise minIP slabs. These minIP images thereby reveal the continuity of tortuous veins across the slices

while attenuating the signal coming from the brain tissue<sup>[4]</sup>. On magnitude images, the longer TE of the SWI sequence (e.g., 40 ms at 1.5 tesla) compared with conventional GE sequences (TE 25 ms) allows for more phase dispersion and T2 shortening of the protons in the local inhomogeneous magnetic field. Thus SWI highlights small changes in susceptibility across a voxel as signal intensity loss. A low flip angle can keep the CSF brighter than the surrounding parenchyma. Consequently, the magnitude image highlights areas with short T2\* and leads to lower signal in major veins due to the presence of deoxyhemoglobin<sup>[6]</sup>. SWI sequence parameters for 1.5 and 3 Tesla Siemens (Erlangen, Germany) and Philips (the Netherlands) magnets are shown in Tables 1-4.

Paramagnetic materials have at least one unpaired electron in the system, but diamagnetic materials have all their electrons paired. Diamagnetic materials are repelled by a magnetic field; an applied magnetic field creates an induced magnetic field in them in the opposite direction, causing a repulsive force. In contrast, paramagnetic and ferromagnetic materials are attracted by a magnetic field. Oxyhemoglobin is diamagnetic in nature, whereas deoxyhemoglobin is paramagnetic. The paramagnetic deoxyhemoglobin serves as an intrinsic contrast agent on SWI sequences, and is low in signal. This causes magnetic field inhomogeneity due to two effects: A reduction of T2\* and a phase difference between the vessel and its surrounding tissue. This property also forms the basic principle for blood oxygen level dependent functional and venographic imaging.

Paramagnetic substances display positive phase shift in left-handed MR systems such as the Avanto system of Siemens magnets (Erlangen, Germany). Hence, the phase images are particularly useful for differentiating between paramagnetic susceptibility effects of blood products such as deoxygenated hemoglobin, intracellular methemoglobin, hemosiderin and ferritin (positive shift) and diamagnetic effects of calcium (negative or no shift)<sup>[7,8]</sup>. Unfortunately, ferrococalcification may lead to confusing signal intensity patterns as even basal ganglia "calcification" is often a mixture of paramagnetic iron and diamagnetic calcium. Yamada *et al*<sup>[8]</sup> demonstrated that all basal ganglia calcifications show a paramagnetic susceptibility effect, whereas other calcifications located outside the basal ganglia (such as choroid plexus or dural calcifications) exhibit exclusively a diamagnetic susceptibility effect. Iron accumulation in brain not only occurs in aging but is also encountered in diverse neurodegenerative diseases.

SWI sequences have some intrinsic disadvantages. Undesirable magnetic susceptibility sources that cause artifacts occurring at air-tissue interfaces such as the areas adjacent to the temporal bone and sinuses limit investigation of these regions. Also the blooming artifact, a useful sign for detecting sources of field inhomogeneity, may sometimes lead to extreme tissue signal cancellation and loss of anatomical borders<sup>[4]</sup>.

**Table 1** Susceptibility weighted imaging sequence parameters for 1.5 T Siemens Magnetom Avanto syngo magnet

Slab group 1	
Slabs	1
Dist. factor	20%
Position	L0.0 A16.0 H37.8
Orientation	T > C-6.9
Phase enc. dir.	R >> L
Rotation	90.00 deg
Phase oversampling	0%
Slabe oversampling	23.10%
Slices per slab	104
FoV read	230 mm
FoV phase	75%
Slice thickness	1.50 mm
TR	28 ms
TE	20.00 ms
Averages	1
Concatenations	1
Filter	Prescan normalize
Matrix size	256 × 256
TA	4.44
PAT	2
Voxel size	1.0 mm × 0.9 mm × 1.5 mm
Flip angle	15 deg
Dimension	3D
Bandwidth	120 Hz/Px
Slice resolution	100%
Coil elements	HE1-4

**Table 2** Susceptibility weighted imaging sequence parameters for 3 T Siemens Magnetom TrioTim syngo magnet

Slab group 1	
Slabs	1
Dist. factor	20%
Position	L0.0 A16.0 H37.8
Orientation	T > C-6.9
Phase enc. dir.	R >> L
Rotation	90.00 deg
Phase oversampling	0%
Slabe oversampling	23.10%
Slices per slab	104
FoV read	230 mm
FoV phase	75%
Slice thickness	1.50 mm
TR	28 ms
TE	20.00 ms
Averages	1
Concatenations	1
Filter	Prescan normalize
Matrix size	256 × 256
TA	4.44
PAT	2
Voxel size	1.0 mm × 0.9 mm × 1.5 mm
Flip angle	15 deg
Dimension	3D
Bandwidth	120 Hz/Px
Slice resolution	100%
Coil elements	HEA; HEP; NE1, 2

## CLINICAL APPLICATIONS

### Cerebral amyloid angiopathy

Cerebral amyloid angiopathy (CAA) is a small vessel disease characterized by amyloid  $\beta$  protein deposition within the cerebral arterioles leading to fibrinoid necrosis and vessel fragility. CAA causes microhemorrhages in and around the arteriole vessel wall extending into the parenchyma<sup>[9]</sup>. CAA is a major cause of primary lobar intracranial hemorrhage and cerebral microhemorrhages in the elderly<sup>[10]</sup>. CT and routine MRI techniques are usually not able to detect cerebral microbleeds; however, SWI with its unique sensitivity to susceptibility effects, clearly demonstrates lobar and microhemorrhages predominantly in the frontal and parietal cortical and subcortical regions (Figure 1). In contrast, microhemorrhages resulting from hypertensive or atherosclerotic microangiopathy have a predilection of deep gray matter or the infratentorial location (Figure 2). CAA is also manifested by white matter hyperintensities on MRI sequences which may be accompanied clinically by cognitive impairment<sup>[11]</sup>. Detection of two or more lobar hemorrhages of any duration, high signal intensity changes in the white matter and multiple cerebral microbleeds at the corticomedullary junction are highly suspicious for CAA (10) (Figure 1). Linn *et al*<sup>[12]</sup> have highlighted the presence of hemosiderosis on the pial surface of the brain, likely from the leakage of blood products from repetitive superficial hemorrhages in as much as 35% of CAA cases.

### Hypertensive cerebral angiopathy

Hypertensive cerebral angiopathy may also be char-

acterized by multiple silent cerebral microhemorrhages. Unlike CAA, cerebral microhemorrhages associated with chronic systemic hypertension are more commonly found in the thalamus, basal ganglia, cerebellum and pons<sup>[10]</sup> (Figure 2). These hypertensive cerebral microhemorrhages are a risk factor for development of a subsequent intracerebral macrohematomas/lobar hemorrhages<sup>[13]</sup>. The number of cerebral microhemorrhages corresponds also with blood pressure levels. Such micro- and macrohemorrhages are exquisitely well-demonstrated by SWI particularly with acute deoxyhemoglobin or chronic hemosiderin.

## TRAUMATIC BRAIN INJURIES

Diffuse axonal injury (DAI) is a type of traumatic brain injury, in which torsional forces generated by rapid acceleration or deceleration of the head cause shearing of axons. Areas most vulnerable to shear injury include the cerebral gray-white matter junction, splenium of the corpus callosum, basal ganglia and dorsolateral brainstem<sup>[10]</sup>. The extent of the axonal injury has been shown to correlate with a poor prognosis, as do parenchymal hemorrhages<sup>[14]</sup>. Recent studies have shown that SWI is more sensitive than CT or GE sequences in terms of detecting suspected hemorrhagic DAI<sup>[15]</sup>. Most DAI patients have small punctate hemorrhages located in the deep subcortical white matter<sup>[16]</sup> (Figure 3). Tong *et al*<sup>[17,18]</sup> and Babikian *et al*<sup>[19]</sup> demonstrated that SWI is 3-6 times more sensitive than T2\* GE sequences in terms of detecting the number, size, volume and distribution of hemorrhagic lesions seen in DAI cases.

**Table 3** Susceptibility weighted imaging sequence parameters for 1.5 T Philips Achieva magnet

FoV read	230 mm
Slice thickness	5 mm
Gap	0
TR	35 ms
TE	50 ms
Matrix size	256 × 512
TA	5.15
Flip angle	15 deg
Coil elements	8 channel SENSE head coil

**Table 4** Susceptibility weighted imaging sequence parameters for 3 T Philips Achieva magnet

FoV read	230 mm
Slice thickness	5 mm
Gap	0
TR	23 ms
TE	20 ms
Matrix size	218 × 127
TA	4.08
Flip angle	10 deg
Coil elements	8 channel SENSE head coil

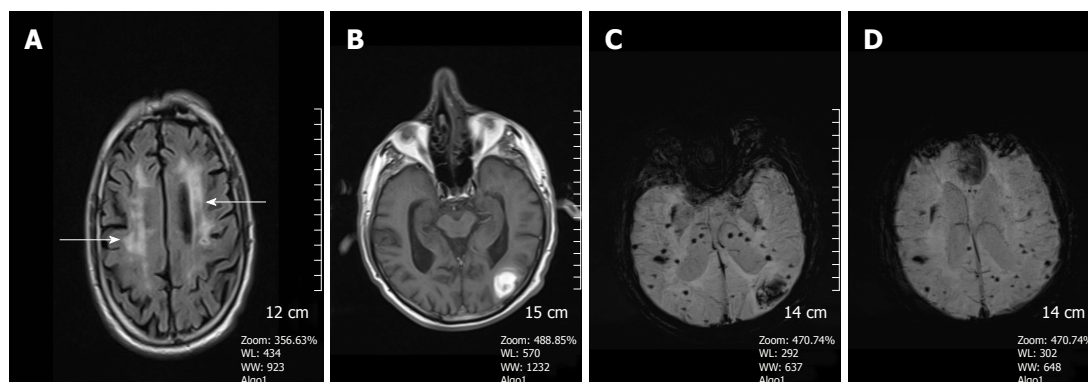


**Figure 1** A 68-year-old man with cerebral amyloid angiopathy. A: Axial FLAIR image demonstrates periventricular confluent hyperintense regions; B: Axial T1 weighted SE image shows high signal intensity subacute hemorrhage in the left occipital lobe; C and D: On SWI minIP images, hemorrhage is depicted as a hypointense signal intensity lesion and, in addition to the left occipital lobar hemorrhage, one can see multiple microhemorrhagic lesions in the cortical and subcortical white matter from cerebral amyloid angiopathy. SWI: Susceptibility weighted imaging; minIP: Minimum intensity projection algorithm; SE: Spin echo.

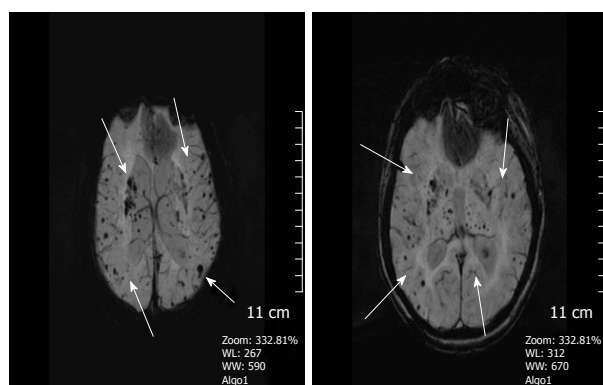


**Figure 2** A 45-year-old woman with long standing chronic hypertension. SWI minIP images depicts numerous microhemorrhages in the deep basal ganglia, thalami, and subcortical white matter regions, typical of hypertensive microangiopathy. SWI: Susceptibility weighted imaging.

Because of this, the previously held concept of “non-hemorrhagic shearing injury” has largely been debunked. Those formerly “bland lesions” of DAI are now shown to have microbleeds on SWI. Brain stem involvement in DAI patients is also a very important predictor that determines the long-term outcome<sup>[20]</sup>. Mittal *et al*<sup>[16]</sup> demonstrated that SWI was more helpful in detecting traumatic lesions occurring in the brainstem than any other MRI sequence, and revealed intraventricular and subarachnoid hemorrhage, invisible on CT. Long term

hemosiderosis from recurrent traumatic bleeds (which may occur in non-accidental trauma) is also best detected on SWI. Epidural and subdural hematomas can also be demonstrated well on SWI sequences as long as air-bone interfaces do not lead to masking artifacts.

## CNS VASCULAR MALFORMATIONS

True arteriovascular malformations (AVMs) usually are present at birth and can become large with time. These AVMs are characterized by their high-flow and therefore can usually be detected by conventional MRI/MR angiography techniques. In contrast, low-flow vascular malformations including cerebral cavernous malformations (CCMs), developmental venous anomalies (DVAs) and CaTe (capillary telangiectasias) may be inapparent on fast spin echo (FSE) MRI/MR angiography techniques because they mainly contain slow-flow small vessels. Although T2\* weighted GE imaging is capable of detecting small venous structures and hemosiderin deposition in cavernomas and CaTes, the incorporation of the magnitude and phase information in SWI provides improved sensitivity for identifying low-flow vascular malformations that are undetectable on GE sequences<sup>[21,22]</sup>. Lee *et al*<sup>[21]</sup> showed that SWI is the ideal imaging sequence for screening patients who have a high clinical suspicion of low-flow vascular malformations. These lesions may be responsible for cryptogenic

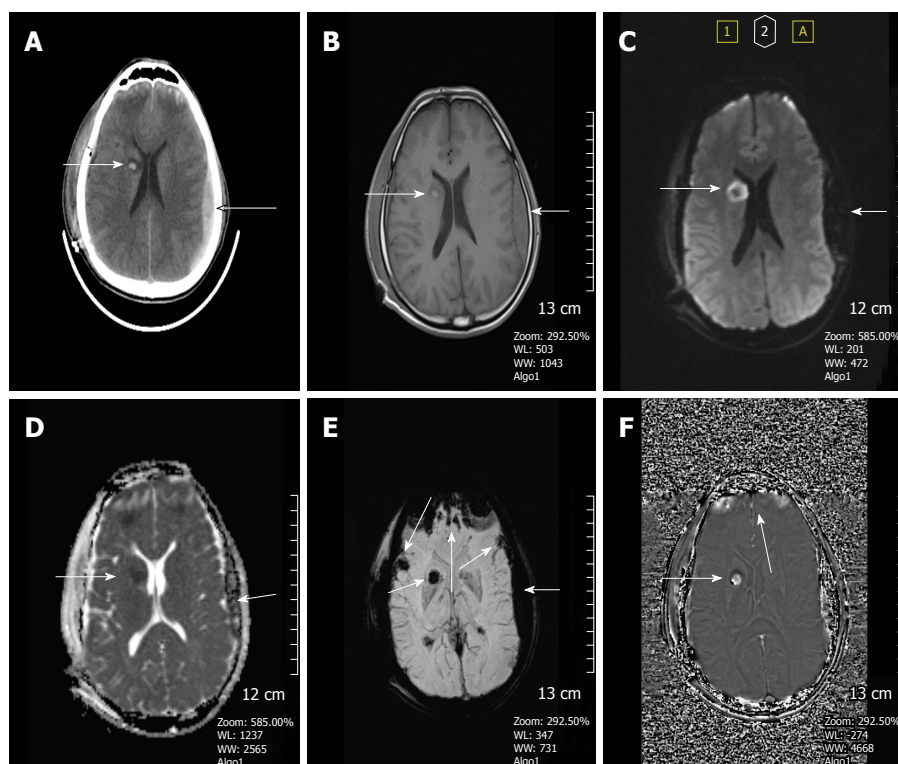


**Figure 3** A 37-year-old man who had an accident was in coma after traumatic brain injury. A: On the non-contrast CT image, bilateral frontal subcortical and right basal ganglia hyperdense hemorrhagic foci with surrounding hypodense edema are seen consistent with diffuse axonal injury. Also left parieto-temporal subdural hemorrhage is present. Post-op changes are present on the right with a tiny frontal subdural hematoma; B: SE T1W image, can only reveal hyperintense right basal ganglia hemorrhagic lesion with surrounding hypointense edema and left subdural hemorrhage, but can not demonstrate the other parenchymal lesions; C: Diffusion weighted image (DWI) reveals hyperintense caudate lesions; D: Apparent diffusion coefficients (ADC) map demonstrates restricted diffusion within the lesions; E: SWI minIP image, clearly depicts multiple frontal cortical and subcortical and also right basal ganglion microhemorrhages better than those of CT and T1W MR image. The bilateral subdural hematomas are nearly as dark as the cortical bone; F: Phase contrast SWI image, hemorrhagic lesions show a bright/positive shift effect on phase image, due to paramagnetic susceptibility effect. SWI: Susceptibility weighted imaging; minIP: Minimum intensity projection algorithm; SE: Spin echo.

epilepsy, recurrent subarachnoid hemorrhage and/or hemosiderosis, and hemorrhagic injury to cranial nerves. Because the incidence of hemorrhage from occult cerebrovascular malformations is contingent on whether they have ever bled, using SWI to detect previous bleeding helps prognosticate on future risk<sup>[23]</sup>.

CCMs are composed of abnormally enlarged capillary cavities surrounded by a single layer of endothelium without intervening with brain parenchyma and comprise 10%-20% of all cerebrovascular malformations<sup>[24]</sup>. The MRI findings of CCMs are variable, depending on the presence of calcification and hemorrhage within the lesions, but they typically show a mixed signal intensity, usually recognized as "popcorn-like" with a central reticulated core surrounded by a peripheral rim of hemosiderin<sup>[15]</sup> (Figure 4). Since recurrent microhemorrhages occur in the CCM lesions, they may contain deoxyhemoglobin acutely or hemosiderin chronically, both dark on SWI<sup>[25,26]</sup> (Figure 5). Symptomatic, growing and recurrently hemorrhagic CCMs are considered for surgical resection.

DVAs are the most common type of cerebral vascular malformations ( $\leq 60\%$ ) and are often discovered incidentally during routine MRI examinations<sup>[27]</sup>. A DVA consists of radially arranged venous structures converging to a centrally located venous trunk, which drains normal brain

parenchyma<sup>[28]</sup>. They are mainly asymptomatic lesions, do not often bleed, and neurosurgical intervention is largely contraindicated due to the risk of venous infarction<sup>[29]</sup>. However, they have a high association with other vascular malformations, especially CCMs. SWI better shows the collector (head of Medusa) and deep medullary veins (snake hair of Medusa) than T1W contrast enhanced images by virtue of the low intensity of the dark veins on miniIP images (Figure 6).

CaTcs are asymptomatic small vascular malformations typically ranging from several millimeters to 2 cm in size, primarily found in the pons. They may occur sporadically or may be seen with syndromes like hereditary hemorrhagic telangiectasia or after radiation therapy<sup>[30]</sup>. They are characterized by faint contrast enhancement on T1W images and therefore can be easily missed. On SWI, they can be readily identified as hypointense lesions, from deoxyhemoglobin or hemosiderin deposited in this low-flow vascular malformation (Figure 7).

Sturge-Weber syndrome (SWS) is a neurocutaneous disorder, typically seen in children and characterized by a cutaneous angioma, glaucoma and leptomeningeal venous angiomatosis<sup>[31]</sup>. The imaging findings consist of unilateral cerebral atrophy, cortical "tram-track" calcifications, impaired cortical venous outflow and abnormal deep



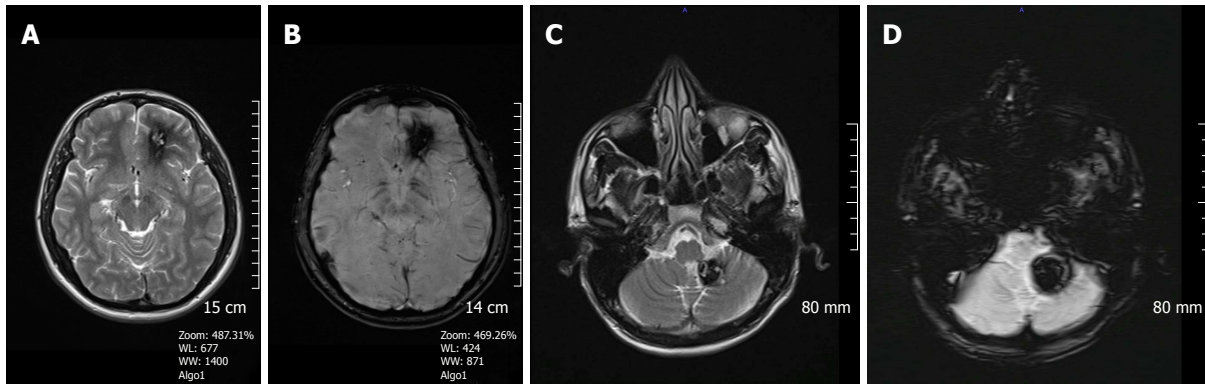


**Figure 4** A 21-year-old man with left frontal cavernous malformation. A: On the axial FSE T2W image, a left frontal cavernous malformation is seen with typical pop-corn appearance, surrounded by a thick hemosiderin rim; B: SWI shows prominent blooming artifact due to paramagnetic effect. Another patient is a 39-year-old man with left cerebellar tonsil cavernous malformation; C: Axial FSE T2W image, clearly depicts the cavernous malformation consisting of a high signal intensity core and a peripheral low signal intensity hemosiderin; D: On SWI, the lesion is more conspicuous. Note how the brighter central areas on the T2WI are obscured by the susceptibility artifact. SWI: Susceptibility weighted imaging; FSE: Fast spin echo.

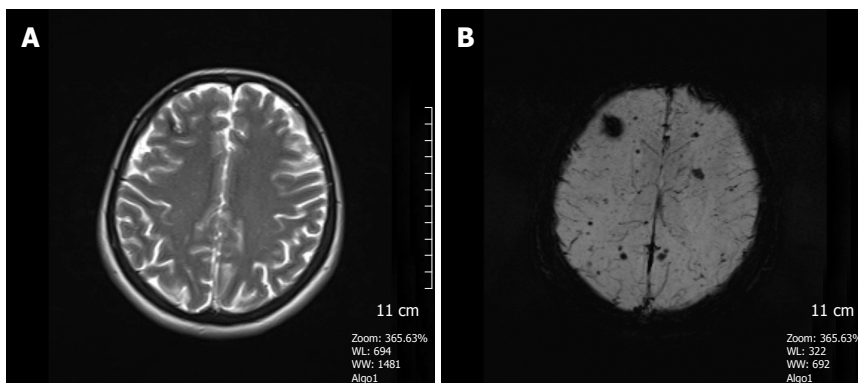


**Figure 5** A 41-year-old woman who had a history of familial cavernous malformation underwent magnetic resonance imaging screening. A: Axial FSE T2W image, a right frontal subcortical small cavernous malformation is seen on this image; B: SWI minIP image, numerous tiny cavernous malformations throughout the brain parenchyma is detected. FSE T2W image is unable to show these lesions. The patient was considered to have familial cerebral cavernous malformation. SWI: Susceptibility weighted imaging; FSE: Fast spin echo.

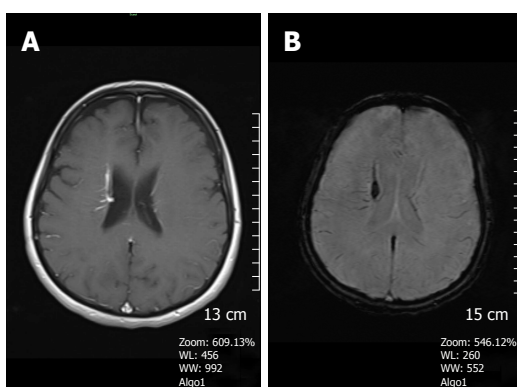


**Figure 6** A 62-year-old woman complaining of long-term headache attacks. A: Axial post-contrast T1W image shows contrast-enhanced dilated medullary veins which seem to converge into a dilated transcortical collector vein in the right periventricular region consistent with developmental venous anomaly; B: Axial SWI minIP image, has an excellent agreement with former image, revealing classical caput medusae appearance. SWI: Susceptibility weighted imaging; minIP: Minimum intensity projection algorithm.

venous collaterals. SWI has been found to be superior to post gadolinium-enhanced T1WI in characterizing calcification, abnormal periventricular and transmedullary

veins, cortical gyriform hypointensities and gray-white matter abnormalities (Figure 8)<sup>[22]</sup>, but enhanced T1W images depict the leptomeningeal angiomas and enlarged choroid plexus more clearly.

### Cerebral venous sinus thrombosis and venous infarction

Patients with cerebral venous sinus thrombosis (CVST) may present with headaches or non-specific signs due to increased intracranial pressure (ICP). Remaining undiagnosed, it can become deadly if it progresses to malignant increased ICP<sup>[32]</sup>. An acute CVST shows deoxyhemoglobin in the involved veins, seen as prominent hypointense signal intensity areas with "blooming" artifact on SWI (Figure 9). SWI may demonstrate engorgement of the venous system as an early sign of CVST and can also show the associated parenchymal hemorrhage which occurs in 73% of venous infarctions<sup>[33]</sup>.

### ARTERIAL STROKE

Acute cerebral infarct with or without hemorrhage occurs due to thromboembolism or atherosclerotic stenosis of a vessel. Vascular occlusion causes a susceptibility change

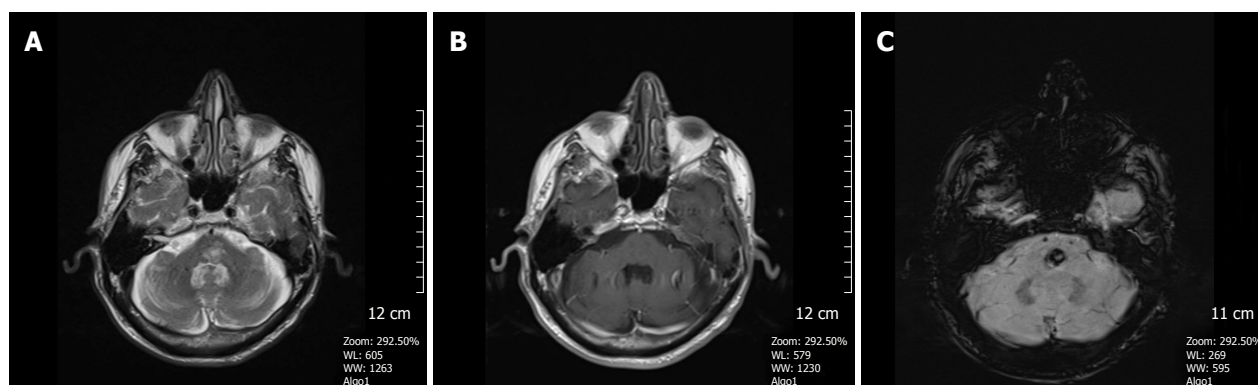


**Figure 7** A 65-year-old man with incidentally discovered capillary telangiectasia in the pons. A: Axial FSE T2W image shows a hyperintense lesion located in the central pons; B: Axial contrast-enhanced T1W image reveals very little contrast enhancement in the lesion; C: SWI image demonstrates a markedly hypointense lesion in the pons indicating a capillary telangiectasia based on its location and size. SWI: Susceptibility weighted imaging; FSE: Fast spin echo.

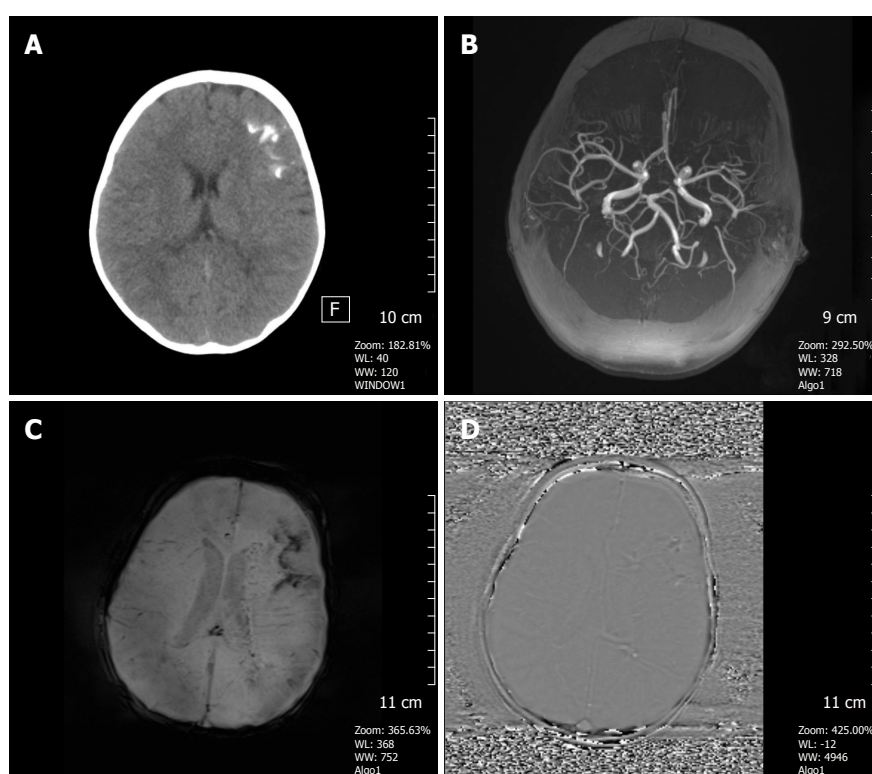


**Figure 8** A 3-year-old girl with Sturge-Weber syndrome. A: Non-contrast CT image shows hyperdense tram-track calcifications along the left frontal gyri; B: Axial MIP TOF MRA shows a normal cranial angiogram; C: Axial SWI minIP image, hypointense gyral calcification is clearly depicted, also deep abnormal transmedullary veins are visible; D: SWI phase image confirms these calcifications as low signal intensity areas. SWI: Susceptibility weighted imaging; minIP: Minimum intensity projection algorithm.

by decreasing the arterial flow, and increases pooling of deoxygenated blood, thus leading to a high concentration of deoxyhemoglobin<sup>[34]</sup>. In the setting of acute stroke, such conversion to deoxyhemoglobin can occur as early as 2 h after the onset of symptoms.

In the setting of stroke, SWI assists in identifying: (1) Hemorrhages within the infarct region, thus enabling the differentiation of a hemorrhagic from a bland and ischemic stroke. Many studies have also proven that SWI is more sensitive in revealing hemorrhage within the acute infarct regions than CT and 2D GE

T2\* weighted sequences<sup>[35,36]</sup>. SWI can also detect acute subarachnoid hemorrhage and is very sensitive to subacute and chronic subarachnoid hemorrhages, sometimes missed by CT and FLAIR<sup>[3]</sup> (Figure 10); (2) Prominent hypointense draining veins within areas of impaired perfusion (Figure 11). The visualization of these prominent veins allows for the identification of diffusion-perfusion mismatch representing penumbral brain tissue in a different fashion than current perfusion weighted imaging techniques<sup>[16]</sup>. The oxygen extraction fraction (OEF) which reflects the ratio of deoxyhemoglobin to

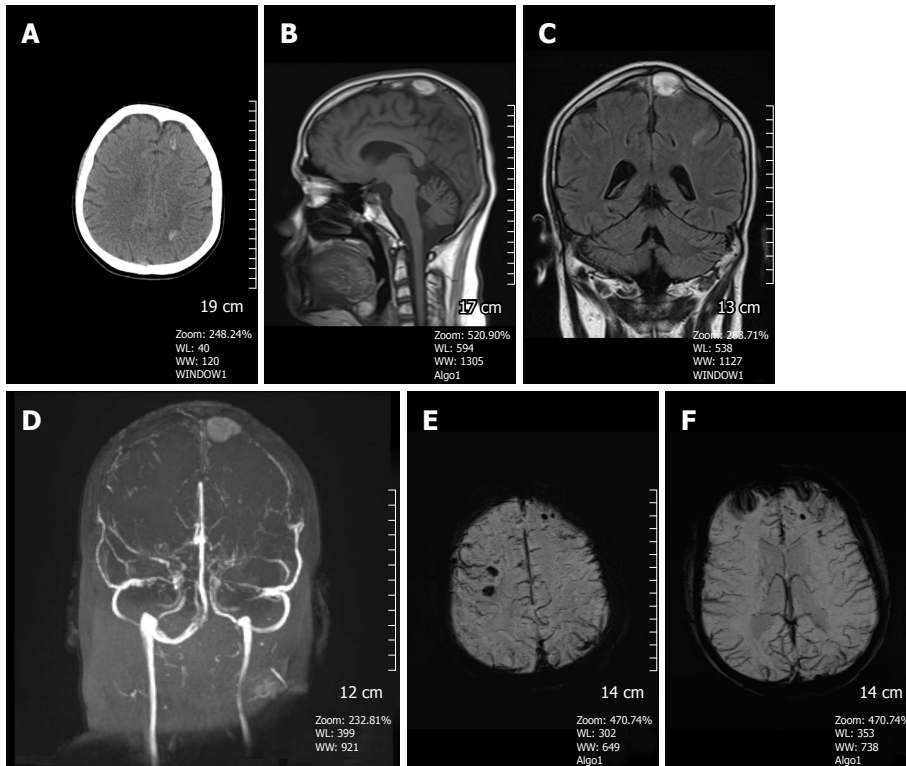


**Figure 9** A 16-year-old man presented with superior sagittal sinus thrombosis. A: Non-contrast CT image shows hyperdense hemorrhagic foci in the left frontal and left parietal lobe at the convexity level (arrows); B: On the sagittal T1W image, a hyperintense thrombus is detected in the superior sagittal sinus; C: Coronal FSE T2W image, thrombus again shows hyperintense signal intensity; D: Time of flight non-contrast MR venography, absence of normal venous flow and accompanying thrombus are clearly depicted; E and F: SWI minIP images demonstrates hypointense microhemorrhages in the brain parenchyma with diffuse dilated venous structures indicating venous engorgement due to venous hypertension. SWI: Susceptibility weighted imaging; minIP: Minimum intensity projection algorithm.

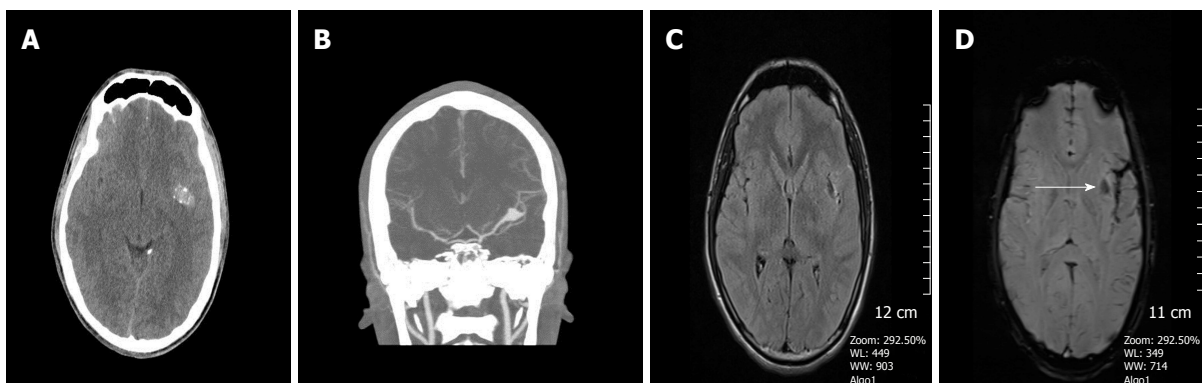


**Figure 10** An 18-year-old man presenting with drastic headache and dizziness. A: Non-contrast CT image reveals a partially calcified hyperdense lesion suspicious for left MCA aneurysm versus cavernoma; B: CT angiography demonstrates a left MCA M1 distal segment aneurysm; C: FLAIR image, left sylvian fissure seems unremarkable with no hemorrhage seen; D: SWI magnitude image shows hypointense acute subarachnoid hemorrhage along the left sylvian fissure. Subinsular low intensity is at edge of aneurysm (arrow). SWI: Susceptibility weighted imaging.

oxyhemoglobin in the capillaries and veins, is significantly increased in the penumbra following occlusion of the artery. This high OEF in cortical veins is presumably responsible for the increased conspicuity in the infarct region<sup>[30,36]</sup>; (3) Acute intra-arterial thrombus: The susceptibility vessel sign (SVS) is defined as the presence of hypointensity from acute deoxyhemoglobin thrombus within the intracranial arteries in which the diameter of the hypointense vessel exceeds the contralateral vessel diameter<sup>[37,38]</sup> (Figures 12 and 13). Lingegowda *et al.*<sup>[39]</sup>

found an 82% sensitivity and 100% specificity for the SVS in the determination of all acute major intracranial occlusions. They also showed that SVS is more sensitive and specific than the hyperdense artery sign on CT<sup>[40,41]</sup> and the hyperintense vessel sign on FLAIR images for intracranial artery occlusions. Huang *et al.*<sup>[42]</sup> found that patients with negative prominent veins and positive susceptibility vessel sign exhibited poor outcomes; and (4) Hemorrhagic transformation of acute ischemic infarction: Approximately 20%-40% of patients bleed



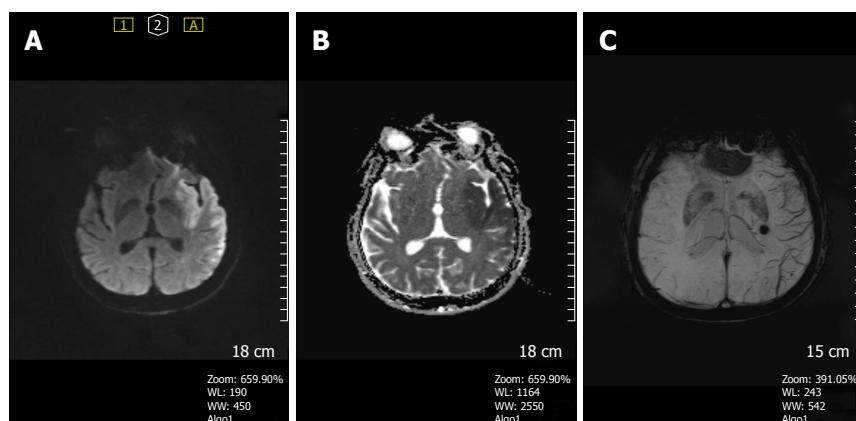


**Figure 11** A 38-year-old man complaining of right side weakness. A: DWI shows hyperintense lesion in the left temporo-insular region; B: ADC map reveals restricted diffusion in the corresponding area indicating a left MCA acute infarct; C: SWI minIP image, prominent cortical veins are seen within the left MCA territory reflecting relatively increased deoxyhemoglobin concentration in the ischemic region. Incidental cavernoma in left thalamus is seen. SWI: Susceptibility weighted imaging; minIP: Minimum intensity projection algorithm; DWI: Diffusion weighted image; ADC: Apparent diffusion coefficients.

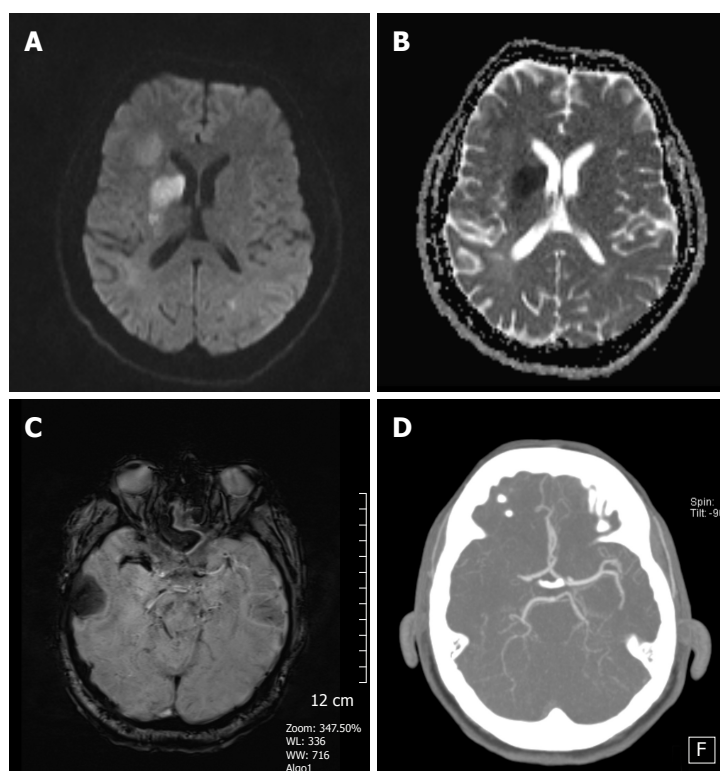


**Figure 12** A 68-year-old woman with right lenticulostriate acute infarct. A: DWI reveals high signal intensity lesion in the right caudate nucleus head and lentiform nucleus region; B: ADC map shows restricted diffusion consistent with an acute infarct; C: Non-contrast CT image, hyperdense artery sign is seen along the right MCA artery; D: SWI magnitude image shows susceptibility vessel sign in the same region corresponding to the CT image indicating an acute thrombus. SWI: Susceptibility weighted imaging; DWI: Diffusion weighted image; ADC: Apparent diffusion coefficients; MCA: Middle cerebral artery.

within the first week after a stroke<sup>[43]</sup> (Figure 14). Old microhemorrhages in a stroke patient may presage the vulnerability of the vascular system<sup>[44]</sup>. In patients with a small number of microhemorrhages (< 5), thrombolytic therapy can be applied safely, whereas patients with large numbers of microhemorrhages (> 5) have a great risk for potential hemorrhagic transformation from thrombolytic therapy<sup>[45-49]</sup>. Huang *et al.*<sup>[42]</sup> showed that microhemorrhages were significantly associated with later hemorrhagic transformation. SWI is able to

detect microhemorrhages within the infarct region more accurately than T2\* weighted GE sequences.

## NEURODEGENERATIVE DISEASES

It is widely accepted that iron deposition in the brain increases with normal aging, particularly in the basal ganglia region primarily in the form of ferritin and ferrocaldinosis (Figure 15). Increased iron levels in the CNS are encountered in a variety of neurodegenerative

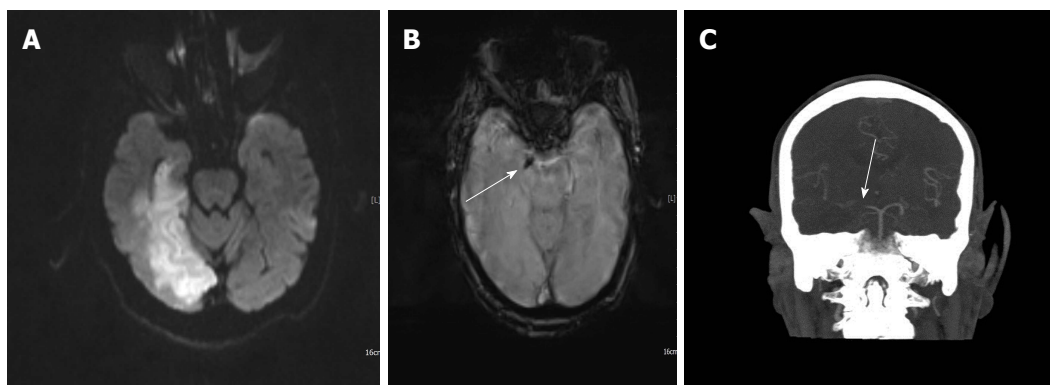


**Figure 13** An 87-year-old woman with right posterior cerebral artery infarct. A: DWI shows right temporo-occipital PCA territory infarct; B: SWI magnitude image shows right PCA P1 segment susceptibility sign; C: Coronal CT MIP angiography image confirms right proximal PCA occlusion. SWI: Susceptibility weighted imaging; PCA: Posterior cerebral artery; DWI: Diffusion weighted image.

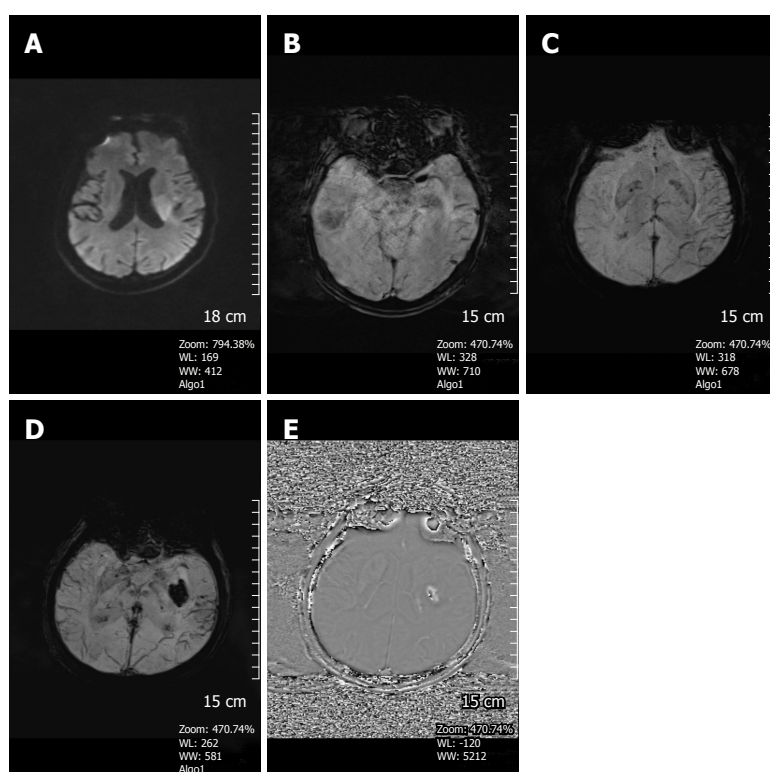


**Figure 14** A 50-year-old man patient with acute left middle cerebral artery infarct. A: DWI, showing a left periventricular hyperintense lesion; B: SWI magnitude image detects left MCA susceptibility vessel sign; C: SWI minIP image reveals prominent hypointense veins in the infarct region; D: Three days later, new SWI minIP image shows hemorrhage in the infarct area indicating development of hemorrhagic transformation. There continues to be permanent venous visualization in the left temporal lobe; E: SWI phase image confirms the hemorrhage leading to a positive shift effect. SWI: Susceptibility weighted imaging; PCA: Posterior cerebral artery; DWI: Diffusion weighted image; minIP: Minimum intensity projection algorithm; MCA: Middle cerebral artery.

diseases, superimposed on the normal senescent iron increase<sup>[50,51]</sup> in the globus pallidum, substantia nigra, red nucleus, subthalamic nucleus and dentate nucleus. Increased iron deposition is found in Parkinson's disease, Huntington's disease, Alzheimer's disease, Multiple sclerosis (MS), Amyotrophic lateral sclerosis, Hallervorden-Spatz syndrome, Wilson's Disease (copper) and Pantothenate kinase-associated neurodegeneration (PKAN)<sup>[52]</sup> (Table 5). In neurodegenerative diseases, the ability to measure the amount of ferritin in the brain may help predict prognosis, disease progression and

treatment outcomes.

SWI shows differences in stable and progressive MCI<sup>[57]</sup>. Fourteen percent of controls, 33% of patients with stable MCI and 54% of those with progressive MCI had microhemorrhages. Furthermore, the iron content in the right pallidum and right substantia nigra was greater in progressive MCI than stable MCI.

Barnaure *et al.*<sup>[58]</sup> studied 328 cognitively normal control subjects and 71 patients with MCI using SWI on a 3T magnet to investigate the presence and distribution of cerebral microbleeds. They found no difference be-

**Table 5** Increased iron levels in the central nervous system

Entity	Increased iron location	Ref.
Parkinson's disease	SN, pars compacta, brainstem	[53]
Alzheimer's disease	Hippocampus, GP	[54]
PKAN	GP, SN sparing DN	[55]
Infantile neuroaxonal dystrophy	GP, SN, DN	[55]
Neuroferritinopathy	GP, P, DN with cavitation	[55]
Aceruloplasminemia	BG, thalami with no cavitation	[55]
Huntington's disease	CN, P	[56]
Progressive MCI versus stable MCI	Right GP, SN	[57]
Multiple sclerosis	CN, P and thalamic pulvinar	[60]

CN: Caudate nucleus; GP: Globus Pallidus; P: Putamen; BG: Basal Ganglia; SN: Substantia Nigra; DN: Dentate nucleus; PKAN: Pantothenate kinase-associated neurodegeneration.

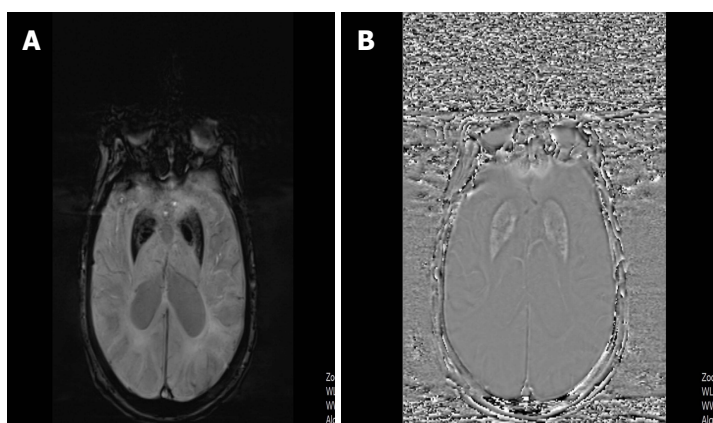


**Figure 15** A 79-year-old woman with Alzheimer's disease. A: SWI minIP image shows hypointense signal intensity in the globus pallidus and putamen indicating increased iron deposition; B: SWI phase image reveals hyperintense signal in the basal ganglia due to the positive shift effect of paramagnetic iron. SWI: Susceptibility weighted imaging; minIP: Minimum intensity projection algorithm.

tween the two groups in terms of cerebral microbleed prevalence, distribution and severity. The patients' cognitive decline over an 18 mo period did not correlate with microbleeds. They concluded that microbleeds do not predict cognitive decline in advanced age.

MS affects both brain and spinal cord and is typically imaged with FLAIR and contrast-enhanced T1W images. The sensitivity of MRI in depicting MS lesions in the brain is demonstrated to be high, but its specificity remains low. SWI helps by revealing the perivenular distribution of the demyelinating lesions by showing the MS plaque surrounding the small veins<sup>[59]</sup>. This has been used to distinguish MS from SAPHO (synovitis, acne, pustulosis, hyperostosis and osteitis) syndrome white matter lesions.

Rudko *et al*<sup>[61]</sup> have shown that the levels of iron deposition in patients with MS correlates better with disability than MS plaque volume. They have also shown increased iron content in patients with clinically isolated syndrome (CIS).

## BRAIN TUMORS

SWI can help in the grading of cerebral tumors because it provides identification of both hemorrhagic and calcified foci inside the tumors and also allows assessment of

the detailed internal angioarchitecture of the tumors. High grade tumors like glioblastomas usually contain a hemorrhagic component (Figure 16)<sup>[3,62-64]</sup>.

Sehgal *et al*<sup>[65]</sup> demonstrated that in the majority of cases, SWI was equivalent to T1W contrast-enhanced images in the grading of gliomas. The criteria used for this comparison were tumor visibility, boundaries, edema, vessels, blood products, internal architecture and image quality. Mittal *et al*<sup>[16]</sup> have showed that high rCBV values on PWI and high choline-creatine ratios on MR spectroscopy found in tumors exhibit a good correlation with evidence of blood products demonstrated within the tumor using SWI.

In assessing brain tumors, calcification is considered as a very important indicator. Calcification is diamagnetic, whereas hemorrhage is paramagnetic, therefore resulting in opposite signal intensities on SWI phase images<sup>[66]</sup>. For the determination of calcification in brain tumors such as oligodendrogliomas, Zulfigar *et al*<sup>[67]</sup> found that adding SWI sequences led to a statistically significant improvement in the sensitivity for the detection of intratumoral calcification by 53% (from 33% to 86%) but no change in specificity.

SWI can also be used to distinguish vestibular schwannomas from cerebellopontine angle meningiomas.

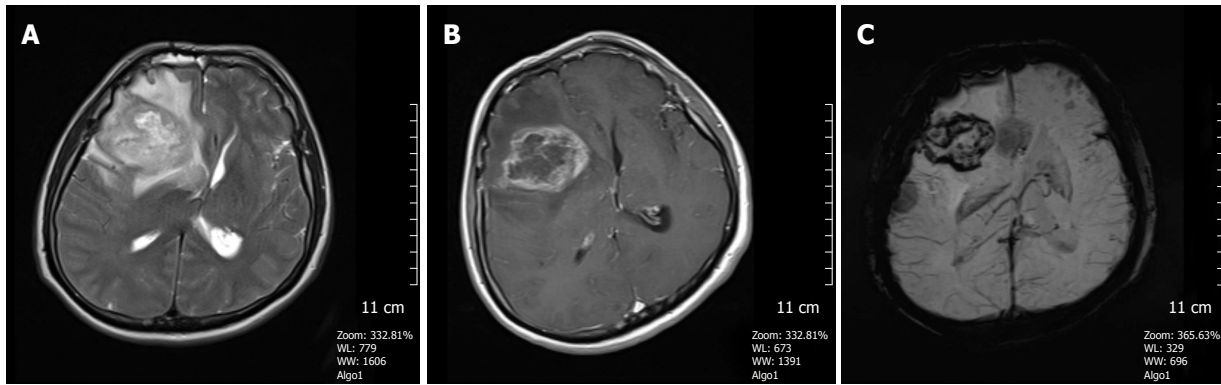


**Figure 16** A 48-year-old man with a history of glioblastoma multiforme. A: FSE T2W image, a heterogenous high signal intensity right frontal lobe mass and surrounding hyperintense infiltrative edema is seen. Tumor is compressing the right lateral ventricle and leading to right to left shift; B: Axial SE T1W contrast- enhanced image, tumor shows heterogenous contrast enhancement; C: SWI minIP image reveals microhemorrhages in the periphery of the tumor indicating a high grade neoplasm. SWI: Susceptibility weighted imaging; minIP: Minimum intensity projection algorithm; FSE: Fast spin echo.

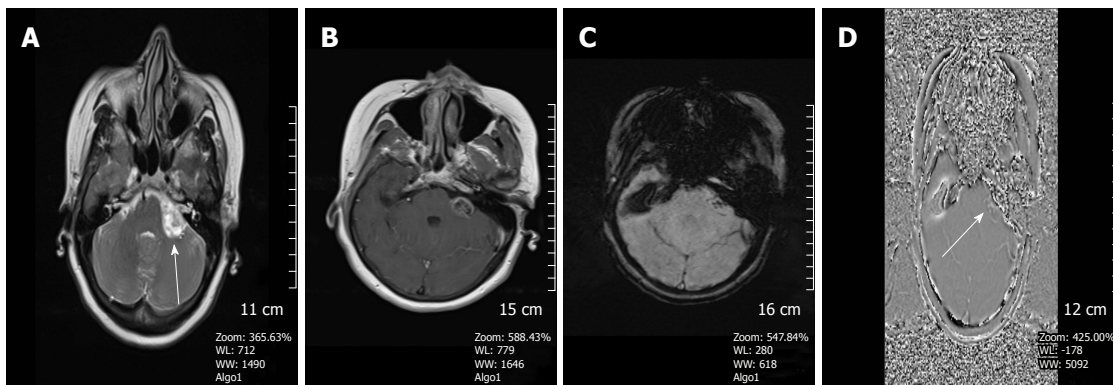


**Figure 17** A 55-year-old woman complaining of left-sided tinnitus. A: Axial FSE T2W image, a heterogenous high signal intensity mass in the left cerebellopontine angle cistern is present; B: On the axial SE T1W contrast- enhanced image, heterogenous contrast enhancement is seen; C: SWI magnitude image reveals punctate hypointense foci within the mass indicating a probable acoustic schwannoma; D: SWI phase image confirms bright microhemorrhages causing a paramagnetic effect. SWI: Susceptibility weighted imaging; FSE: Fast spin echo.

Microhemorrhages occur with schwannomas, not found in the meningiomas<sup>[68]</sup> (Figure 17).

The dual rim sign (hyperintense inner, hypointense outer) from the respiratory burst of bacteria converting hemoglobin to methemoglobin has been shown to differentiate abscesses (present) from glioblastoma (absent) in the face of a ring enhancing mass<sup>[69]</sup>.

## QSM

QSM is a recently developed sophisticated postprocessing technique and numerically solves the inverse source-effect problem to quantify local tissue magnetic susceptibility from the major magnetic field distribution, reflected in the phase images of SWI<sup>[70]</sup>. The mapping of iron can play a crucial role in the setting of many important neurologic disorders. In early Parkinson's disease (PD), iron elevation in the specific brain regions including the substantia nigra is a pathognomonic feature of the disease and this can be measured by QSM<sup>[71]</sup>. He *et al.*<sup>[72]</sup> evaluated 44 early PD patients; susceptibility values within the substantia nigra and red nucleus contralateral to the most affected limb were

elevated compared to a healthy control group. Bilateral substantia nigra magnetic susceptibility showed a positive correlation with disease duration<sup>[72]</sup>.

Acosta-Cabronero *et al.*<sup>[73]</sup> examined 66 patients with idiopathic PD and found increased R2\* and susceptibility values in the substantia nigra, red nucleus, thalamus and globus pallidus. QSM additionally correlated with disease severity in these patients.

Moon *et al.*<sup>[74]</sup> investigated the presence and pattern of brain iron accumulation in vascular dementia (VaD) and Alzheimer's disease (AD) patients by means of QSM. Both in VaD and AD patients significantly higher susceptibility values were found in the caudate nucleus and putamen compared to control subjects. Age and cognitive disease severity of both patient groups were not correlated with increased iron accumulation in their basal ganglia (Figure 18).

Dominguez *et al.*<sup>[75]</sup> measured iron accumulation in the basal ganglia in both premanifest and symptomatic Huntington's disease (HD) patients with QSM. Both groups of patients demonstrated substantially elevated iron content in the caudate nucleus, globus pallidus and putamen compared to normal control subjects. In-



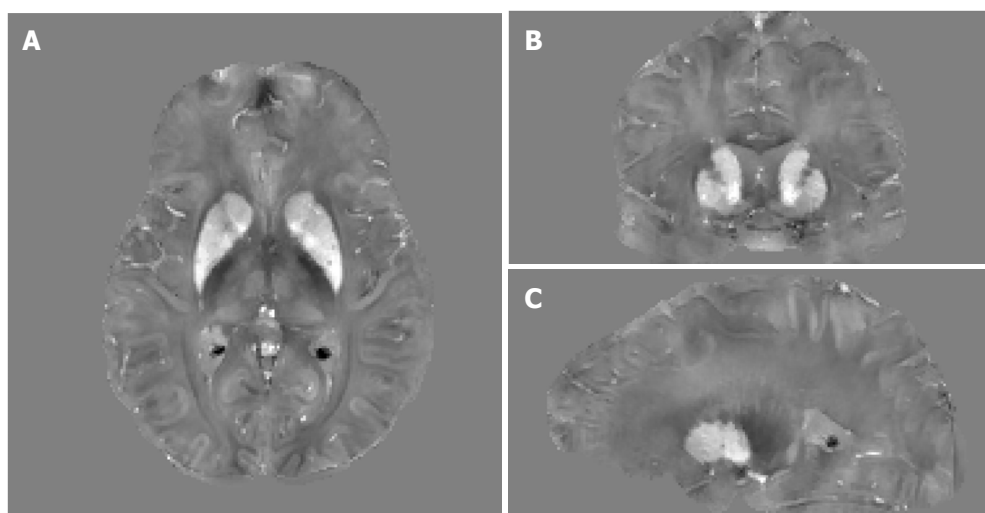


**Figure 18** Example orthogonal views of quantitative susceptibility mapping images of a 41-year-old female premanifest HD patient showing the basal ganglia where increased tissue magnetic susceptibility can be observed in iron-rich gray matter structures such as the caudate nuclei and putamen. Extra iron overload in the striatum in these patients as compared to age-matched controls is believed to be associated with HD pathophysiology. Gray scale is in  $[-0.2, 0.2]$  ppm.

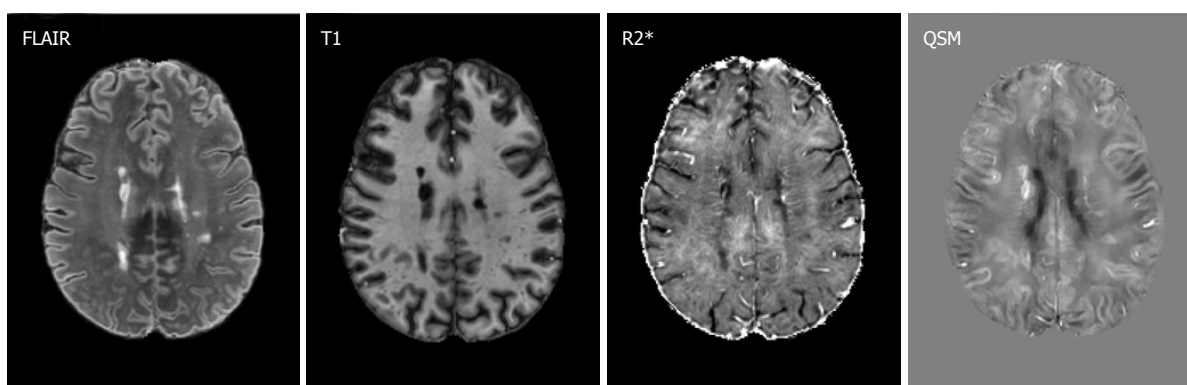


**Figure 19** Example quantitative susceptibility mapping image of a 55-year-old female relapsing-remitting MS patient, shows hyperintense susceptibility MS lesions, and the corresponding FLAIR, T1 and R2\* images. Multiple contrast analysis using R2\* and QSM may be helpful identifying different pathological changes in MS lesions. Gray scale is  $[-0.12, 0.12]$  ppm in QSM image and  $[0, 80]$  Hz in R2\* image. MS data was acquired using similar 7T protocol as the HD study. QSM: Quantitative susceptibility mapping.

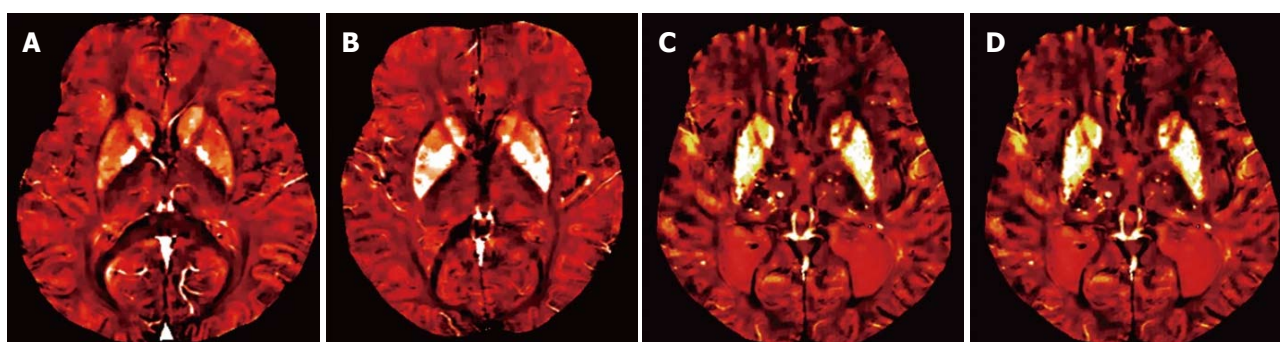


**Figure 20** Increased iron accumulation of caudate and putamen is noted in patients with Alzheimer's disease and vascular dementia as compared with normal subjects.

creased iron levels showed significant correlation with disease severity (Figure 19). QSM is also capable of quantifying elevated iron levels in the motor cortex of amyotrophic lateral sclerosis patients. Furthermore, in Wilson's disease, iron accumulation and quantification can be demonstrated by QSM<sup>[71]</sup>. Iron chelation therapy in PD can be monitored by QSM<sup>[71]</sup>. Walsh *et al.*<sup>[76]</sup> have

shown that the deficits of patients with MS more strongly correlate with QSM values of brain iron content than the MS plaque volume (Figure 20).

## CONCLUSION

SWI is a very useful imaging tool with a variety of ap-

plications in neuroradiology practice and should be included in routine protocols. As demonstrated, it is very helpful in detecting micro-and macro-hemorrhages and delineating cerebral microvasculature and low-flow vascular malformations. It is regarded as a complementary, valuable imaging sequence in the management of stroke patients. It facilitates differentiation of calcium from hemorrhage in the brain. It is helpful in the evaluation of traumatic brain injury patients and aids in the characterization and grading of cerebral tumors. QSM can shed light on many neurodegenerative disorders in a more rigorous statistical way by assessing brain iron content. Further investigations are needed for expanding the roles of SWI and QSM in neuroradiology clinical and research arenas.

## ACKNOWLEDGMENTS

Our thanks to Xu Li, PhD, from Johns Hopkins Medical Institution, Radiology and Radiological Sciences, Baltimore, Maryland, United States, for his support in providing the QSM part figures (18 and 19) of our article. We are also grateful to the Korean Journal of Radiology for their permission of Figure 20.

## REFERENCES

1. **Reichenbach JR**, Venkatesan R, Schillinger DJ, Kido DK, Haacke EM. Small vessels in the human brain: MR venography with deoxyhemoglobin as an intrinsic contrast agent. *Radiology* 1997; **204**: 272-277 [PMID: 9205259 DOI: 10.1148/radiology.204.1.9205259]
2. **Reichenbach JR**, Haacke EM. High-resolution BOLD venographic imaging: a window into brain function. *NMR Biomed* 2001; **14**: 453-467 [PMID: 11746938 DOI: 10.1002/nbm.722]
3. **Thomas B**, Somasundaram S, Thamburaj K, Kesavadas C, Gupta AK, Bodhey NK, Kapilamoorthy TR. Clinical applications of susceptibility weighted MR imaging of the brain - a pictorial review. *Neuroradiology* 2008; **50**: 105-116 [PMID: 17929005 DOI: 10.1007/s00234-007-0316-z]
4. **Gasparotti R**, Pinelli L, Liserre R. New MR sequences in daily practice: susceptibility weighted imaging. A pictorial essay. *Insights Imaging* 2011; **2**: 335-347 [PMID: 22347957 DOI: 10.1007/s13244-011-0086-3]
5. **Haacke EM**, Xu Y, Cheng YC, Reichenbach JR. Susceptibility weighted imaging (SWI). *Magn Reson Med* 2004; **52**: 612-618 [PMID: 15334582 DOI: 10.1002/mrm.20198]
6. **Haacke EM**, Mittal S, Wu Z, Neelavalli J, Cheng YC. Susceptibility-weighted imaging: technical aspects and clinical applications, part 1. *AJNR Am J Neuroradiol* 2009; **30**: 19-30 [PMID: 19039041 DOI: 10.3174/ajnr.A1400]
7. **Rauscher A**, Sedlacik J, Barth M, Mentzel HJ, Reichenbach JR. Magnetic susceptibility-weighted MR phase imaging of the human brain. *AJNR Am J Neuroradiol* 2005; **26**: 736-742 [PMID: 15814914]
8. **Yamada N**, Imakita S, Sakuma T, Takamiya M. Intracranial calcification on gradient-echo phase image: depiction of diamagnetic susceptibility. *Radiology* 1996; **198**: 171-178 [PMID: 8539373 DOI: 10.1148/radiology.198.1.8539373]
9. **Greenberg SM**, Eng JA, Ning M, Smith EE, Rosand J. Hemorrhage burden predicts recurrent intracerebral hemorrhage after lobar hemorrhage. *Stroke* 2004; **35**: 1415-1420 [PMID: 15073385 DOI: 10.1161/01.STR.0000126807.69758.0e]
10. **Blitstein MK**, Tung GA. MRI of cerebral microhemorrhages. *AJR Am J Roentgenol* 2007; **189**: 720-725 [PMID: 17715122 DOI: 10.2214/AJR.07.2249]
11. **Smith EE**, Gurool ME, Eng JA, Engel CR, Nguyen TN, Rosand J, Greenberg SM. White matter lesions, cognition, and recurrent hemorrhage in lobar intracerebral hemorrhage. *Neurology* 2004; **63**: 1606-1612 [PMID: 15534243 DOI: 10.1212/01.WNL.0000142966.22886.20]
12. **Linn J**, Halpin A, Demaerel P, Ruhland J, Giese AD, Dichgans M, van Buchem MA, Bruckmann H, Greenberg SM. Prevalence of superficial siderosis in patients with cerebral amyloid angiopathy. *Neurology* 2010; **74**: 1346-1350 [PMID: 20421578 DOI: 10.1212/WNL.0b013e3181dad605]
13. **Tsushima Y**, Tanizaki Y, Aoki J, Endo K. MR detection of microhemorrhages in neurologically healthy adults. *Neuroradiology* 2002; **44**: 31-36 [PMID: 11942497 DOI: 10.1007/s002340100649]
14. **Medana IM**, Esiri MM. Axonal damage: a key predictor of outcome in human CNS diseases. *Brain* 2003; **126**: 515-530 [PMID: 12566274 DOI: 10.1093/brain/awg061]
15. **Schaefer PW**, Huisman TA, Sorensen AG, Gonzalez RG, Schwamm LH. Diffusion-weighted MR imaging in closed head injury: high correlation with initial glasgow coma scale score and score on modified Rankin scale at discharge. *Radiology* 2004; **233**: 58-66 [PMID: 15304663 DOI: 10.1148/radiol.2323031173]
16. **Mittal S**, Wu Z, Neelavalli J, Haacke EM. Susceptibility-weighted imaging: technical aspects and clinical applications, part 2. *AJNR Am J Neuroradiol* 2009; **30**: 232-252 [PMID: 19131406 DOI: 10.3174/ajnr.A1461]
17. **Tong KA**, Ashwal S, Holshouser BA, Shutter LA, Herigault G, Haacke EM, Kido DK. Hemorrhagic shearing lesions in children and adolescents with posttraumatic diffuse axonal injury: improved detection and initial results. *Radiology* 2003; **227**: 332-339 [PMID: 12732694 DOI: 10.1148/radiol.2272020176]
18. **Tong KA**, Ashwal S, Holshouser BA, Nickerson JP, Wall CJ, Shutter LA, Osterdock RJ, Haacke EM, Kido D. Diffuse axonal injury in children: clinical correlation with hemorrhagic lesions. *Ann Neurol* 2004; **56**: 36-50 [PMID: 15236400 DOI: 10.1002/ana.20123]
19. **Babikian T**, Freier MC, Tong KA, Nickerson JP, Wall CJ, Holshouser BA, Burley T, Riggs ML, Ashwal S. Susceptibility weighted imaging: neuropsychologic outcome and pediatric head injury. *Pediatr Neurol* 2005; **33**: 184-194 [PMID: 16139733 DOI: 10.1016/j.pediatrneurol.2005.03.015]
20. **Mannion RJ**, Cross J, Bradley P, Coles JP, Chatfield D, Carpenter A, Pickard JD, Menon DK, Hutchinson PJ. Mechanism-based MRI classification of traumatic brainstem injury and its relationship to outcome. *J Neurotrauma* 2007; **24**: 128-135 [PMID: 17263676 DOI: 10.1089/neu.2006.0127]
21. **Lee BC**, Vo KD, Kido DK, Mukherjee P, Reichenbach J, Lin W, Yoon MS, Haacke M. MR high-resolution blood oxygenation level-dependent venography of occult (low-flow) vascular lesions. *AJNR Am J Neuroradiol* 1999; **20**: 1239-1242 [PMID: 10472978]
22. **Barnes SR**, Haacke EM. Susceptibility-weighted imaging: clinical angiographic applications. *Magn Reson Imaging Clin N Am* 2009; **17**: 47-61 [PMID: 19364599 DOI: 10.1016/j.mric.2008.12.002]
23. **Yousem DM**, Flamm ES, Grossman RI. Comparison of MR imaging with clinical history in the identification of hemorrhage in patients with cerebral arteriovenous malformations. *AJNR Am J Neuroradiol* 1989; **10**: 1151-1154 [PMID: 2512776]
24. **Lehnhardt FG**, von Smekal U, Rückriem B, Stenzel W, Neveling M, Heiss WD, Jacobs AH. Value of gradient-echo magnetic resonance imaging in the diagnosis of familial cerebral cavernous malformation. *Arch Neurol* 2005; **62**: 653-658 [PMID: 15824268 DOI: 10.1001/archneur.62.4.653]
25. **Cooper AD**, Campeau NG, Meissner I. Susceptibility-weighted imaging in familial cerebral cavernous malformations. *Neurology* 2008; **71**: 382 [PMID: 18663188 DOI: 10.1212/01.wnl.0000319659.86629.c8]
26. **Abla A**, Wait SD, Uschold T, Lekovic GP, Spetzler RF. Developmental venous anomaly, cavernous malformation, and capillary telangiectasia: spectrum of a single disease. *Acta Neurochir (Wien)*

- 2008; **150**: 487-489; discussion 489 [PMID: 18351283 DOI: 10.1007/s00701-008-1570-5]
- 27 **Abe T**, Singer RJ, Marks MP, Norbash AM, Crowley RS, Steinberg GK. Coexistence of occult vascular malformations and developmental venous anomalies in the central nervous system: MR evaluation. *AJNR Am J Neuroradiol* 1998; **19**: 51-57 [PMID: 9432157]
- 28 **Töpper R**, Jürgens E, Reul J, Thron A. Clinical significance of intracranial developmental venous anomalies. *J Neurol Neurosurg Psychiatry* 1999; **67**: 234-238 [PMID: 10407000 DOI: 10.1136/jnnp.67.2.234]
- 29 **Tong KA**, Ashwal S, Obenaus A, Nickerson JP, Kido D, Haacke EM. Susceptibility-weighted MR imaging: a review of clinical applications in children. *AJNR Am J Neuroradiol* 2008; **29**: 9-17 [PMID: 17925363 DOI: 10.3174/ajnr.A0786]
- 30 **Comi AM**. Update on Sturge-Weber syndrome: diagnosis, treatment, quantitative measures, and controversies. *Lymphat Res Biol* 2007; **5**: 257-264 [PMID: 18370916 DOI: 10.1089/lrb.2007.1016]
- 31 **Hinman JM**, Provenzale JM. Hypointense thrombus on T2-weighted MR imaging: a potential pitfall in the diagnosis of dural sinus thrombosis. *Eur J Radiol* 2002; **41**: 147-152 [PMID: 11809544 DOI: 10.1016/S0720-048X(01)00365-5]
- 32 **Mammen EF**. Pathogenesis of venous thrombosis. *Chest* 1992; **102**: 640S-644S [PMID: 1451539 DOI: 10.1378/chest.102.6\_Supplement.640S]
- 33 **Khandelwal N**, Agarwal A, Kochhar R, Bapuraj JR, Singh P, Prabhakar S, Suri S. Comparison of CT venography with MR venography in cerebral sinovenous thrombosis. *AJR Am J Roentgenol* 2006; **187**: 1637-1643 [PMID: 17114562 DOI: 10.2214/AJR.05.1249]
- 34 **Viallon M**, Altrichter S, Pereira VM, Nguyen D, Sekoranta L, Federspiel A, Kulcsar Z, Sztajzel R, Ouared R, Bonvin C, Pfeuffer J, Lövsblad KO. Combined use of pulsed arterial spin-labeling and susceptibility-weighted imaging in stroke at 3T. *Eur Neurol* 2010; **64**: 286-296 [PMID: 20980761 DOI: 10.1159/000321162]
- 35 **Hermier M**, Nighoghossian N. Contribution of susceptibility-weighted imaging to acute stroke assessment. *Stroke* 2004; **35**: 1989-1994 [PMID: 15192245 DOI: 10.1161/01.STR.0000133341.74387.96]
- 36 **Cheng AL**, Batool S, McCreary CR, Lauzon ML, Frayne R, Goyal M, Smith EE. Susceptibility-weighted imaging is more reliable than T2\*-weighted gradient-recalled echo MRI for detecting microbleeds. *Stroke* 2013; **44**: 2782-2786 [PMID: 23920014 DOI: 10.1161/STROKEAHA.113.002267]
- 37 **Flacke S**, Urbach H, Keller E, Träber F, Hartmann A, Textor J, Gieseke J, Block W, Folkers PJ, Schild HH. Middle cerebral artery (MCA) susceptibility sign at susceptibility-based perfusion MR imaging: clinical importance and comparison with hyperdense MCA sign at CT. *Radiology* 2000; **215**: 476-482 [PMID: 10796928 DOI: 10.1148/radiology.215.2.r00ma09476]
- 38 **Rovira A**, Orellana P, Alvarez-Sabín J, Arenillas JF, Aymerich X, Grivé E, Molina C, Rovira-Gols A. Hyperacute ischemic stroke: middle cerebral artery susceptibility sign at echo-planar gradient-echo MR imaging. *Radiology* 2004; **232**: 466-473 [PMID: 15215546 DOI: 10.1148/radiol.2322030273]
- 39 **Linggowda D**, Thomas B, Vaghela V, Hingwala DR, Kesavadas C, Sylaja PN. 'Susceptibility sign' on susceptibility-weighted imaging in acute ischemic stroke. *Neurol India* 2012; **60**: 160-164 [PMID: 22626696 DOI: 10.4103/0028-3886.96389]
- 40 **Kesavadas C**, Santhosh K, Thomas B. Susceptibility weighted imaging in cerebral hypoperfusion-can we predict increased oxygen extraction fraction? *Neuroradiology* 2010; **52**: 1047-1054 [PMID: 20567811 DOI: 10.1007/s00234-010-0733-2]
- 41 **Assouline E**, Benziane K, Reizine D, Guichard JP, Pico F, Merland JJ, Bousser MG, Chabriat H. Intra-arterial thrombus visualized on T2\* gradient echo imaging in acute ischemic stroke. *Cerebrovasc Dis* 2005; **20**: 6-11 [PMID: 15925876 DOI: 10.1159/000086120]
- 42 **Huang P**, Chen CH, Lin WC, Lin RT, Khor GT, Liu CK. Clinical applications of susceptibility weighted imaging in patients with major stroke. *J Neurol* 2012; **259**: 1426-1432 [PMID: 22186853 DOI: 10.1007/s00415-011-6369-2]
- 43 **Kidwell CS**, Saver JL, Villablanca JP, Duckwiler G, Fredieu A, Gough K, Leary MC, Starkman S, Gobin YP, Jahan R, Vespa P, Liebeskind DS, Alger JR, Vinuela F. Magnetic resonance imaging detection of microbleeds before thrombolysis: an emerging application. *Stroke* 2002; **33**: 95-98 [PMID: 11779895 DOI: 10.1161/hs0102.101792]
- 44 **Chalela JA**, Kang DW, Warach S. Multiple cerebral microbleeds: MRI marker of a diffuse hemorrhage-prone state. *J Neuroimaging* 2004; **14**: 54-57 [PMID: 14748209 DOI: 10.1177/1051228403258673]
- 45 **Kesavadas C**, Thomas B, Pendharakar H, Sylaja PN. Susceptibility weighted imaging: does it give information similar to perfusion weighted imaging in acute stroke? *J Neurol* 2011; **258**: 932-934 [PMID: 21116823 DOI: 10.1007/s00415-010-5843-6]
- 46 **Chalela JA**, Kidwell CS, Nentwich LM, Luby M, Butman JA, Demchuk AM, Hill MD, Patronas N, Latour L, Warach S. Magnetic resonance imaging and computed tomography in emergency assessment of patients with suspected acute stroke: a prospective comparison. *Lancet* 2007; **369**: 293-298 [PMID: 17258669 DOI: 10.1016/S0140-6736(07)60151-2]
- 47 **Wycliffe ND**, Choe J, Holshouser B, Oyoyo UE, Haacke EM, Kido DK. Reliability in detection of hemorrhage in acute stroke by a new three-dimensional gradient recalled echo susceptibility-weighted imaging technique compared to computed tomography: a retrospective study. *J Magn Reson Imaging* 2004; **20**: 372-377 [PMID: 15332242 DOI: 10.1002/jmri.20130]
- 48 **von Kummer R**. MRI: the new gold standard for detecting brain hemorrhage? *Stroke* 2002; **33**: 1748-1749 [PMID: 12105345 DOI: 10.1161/01.STR.0000019882.06696.D6]
- 49 **Wintermark M**, Sanelli PC, Albers GW, Bello JA, Derdeyn CP, Hets SW, Johnson MH, Kidwell CS, Lev MH, Liebeskind DS, Rowley HA, Schaefer PW, Sunshine JL, Zaharchuk G, Meltzer CC; American Society of Neuroradiology; American College of Radiology; Society of NeuroInterventional Surgery. Imaging recommendations for acute stroke and transient ischemic attack patients: a joint statement by the American Society of Neuroradiology, the American College of Radiology and the Society of NeuroInterventional Surgery. *J Am Coll Radiol* 2013; **10**: 828-832 [PMID: 23948676 DOI: 10.1016/j.jacr.2013.06.019]
- 50 **Haacke EM**, Cheng NY, House MJ, Liu Q, Neelavalli J, Ogg RJ, Khan A, Ayaz M, Kirsch W, Obenaus A. Imaging iron stores in the brain using magnetic resonance imaging. *Magn Reson Imaging* 2005; **23**: 1-25 [PMID: 15733784 DOI: 10.1016/j.mri.2004.10.001]
- 51 **Harder SL**, Hopp KM, Ward H, Neglio H, Gitlin J, Kido D. Mineralization of the deep gray matter with age: a retrospective review with susceptibility-weighted MR imaging. *AJNR Am J Neuroradiol* 2008; **29**: 176-183 [PMID: 17989376 DOI: 10.3174/ajnr.A0770]
- 52 **Hecht MJ**, Fellner C, Schmid A, Neundörfer B, Fellner FA. Cortical T2 signal shortening in amyotrophic lateral sclerosis is not due to iron deposits. *Neuroradiology* 2005; **47**: 805-808 [PMID: 16175348 DOI: 10.1007/s00234-005-1421-5]
- 53 **Martin WR**, Wieler M, Gee M. Midbrain iron content in early Parkinson disease: a potential biomarker of disease status. *Neurology* 2008; **70**: 1411-1417 [PMID: 18172063 DOI: 10.1212/01.wnl.0000286384.31050.b5]
- 54 **Schenck JF**, Zimmerman EA, Li Z, Adak S, Saha A, Tandon R, Fish KM, Belden C, Gillen RW, Barba A, Henderson DL, Neil W, O'Keefe T. High-field magnetic resonance imaging of brain iron in Alzheimer disease. *Top Magn Reson Imaging* 2006; **17**: 41-50 [PMID: 17179896 DOI: 10.1097/01.rmr.0000245455.59912.40]
- 55 **McNeill A**, Birchall D, Hayflick SJ, Gregory A, Schenk JF, Zimmerman EA, Shang H, Miyajima H, Chinnery PF. T2\* and FSE MRI distinguishes four subtypes of neurodegeneration with brain iron accumulation. *Neurology* 2008; **70**: 1614-1619 [PMID: 18443312 DOI: 10.1212/01.wnl.0000310985.40011.d6]
- 56 **van Bergen JM**, Hua J, Unschuld PG, Lim IA, Jones CK, Margolis RL, Ross CA, van Zijl PC, Li X. Quantitative Susceptibility Mapping Suggests Altered Brain Iron in Premanifest Huntington



- Disease. *AJNR Am J Neuroradiol* 2016; **37**: 789-796 [PMID: 26680466 DOI: 10.3174/ajnr.A4617]
- 57 **Haller S**, Bartsch A, Nguyen D, Rodriguez C, Emch J, Gold G, Lovblad KO, Giannakopoulos P. Cerebral microhemorrhage and iron deposition in mild cognitive impairment: susceptibility-weighted MR imaging assessment. *Radiology* 2010; **257**: 764-773 [PMID: 20923870 DOI: 10.1148/radiol.10100612]
  - 58 **Barnaure I**, Montandon ML, Rodriguez C, Herrmann F, Lövblad KO, Giannakopoulos P, Haller S. Clinicoradiologic Correlations of Cerebral Microbleeds in Advanced Age. *AJNR Am J Neuroradiol* 2017; **38**: 39-45 [PMID: 27686485 DOI: 10.3174/ajnr.A4956]
  - 59 **Tan IL**, van Schijndel RA, Pouwels PJ, van Walderveen MA, Reichenbach JR, Manoliu RA, Barkhof F. MR venography of multiple sclerosis. *AJNR Am J Neuroradiol* 2000; **21**: 1039-1042 [PMID: 10871010]
  - 60 **Haacke EM**, Ayaz M, Khan A, Manova ES, Krishnamurthy B, Gollapalli L, Ciulla C, Kim I, Petersen F, Kirsch W. Establishing a baseline phase behavior in magnetic resonance imaging to determine normal vs. abnormal iron content in the brain. *J Magn Reson Imaging* 2007; **26**: 256-264 [PMID: 17654738 DOI: 10.1002/jmri.22987]
  - 61 **Rudko DA**, Solovey I, Gati JS, Kremenchutzky M, Menon RS. Multiple sclerosis: improved identification of disease-relevant changes in gray and white matter by using susceptibility-based MR imaging. *Radiology* 2014; **272**: 851-864 [PMID: 24828000 DOI: 10.1148/radiol.14132475]
  - 62 **Rauscher A**, Sedlacik J, Fitzek C, Walter B, Hochstetter A, Kalff R, Kaiser WA, Reichenbach JR. High resolution susceptibility weighted MR-imaging of brain tumors during the application of a gaseous agent. *Rofo* 2005; **177**: 1065-1069 [PMID: 16021537 DOI: 10.1055/s-2005-858428]
  - 63 **Sehgal V**, Delproposto Z, Haacke EM, Tong KA, Wycliffe N, Kido DK, Xu Y, Neelavalli J, Haddar D, Reichenbach JR. Clinical applications of neuroimaging with susceptibility-weighted imaging. *J Magn Reson Imaging* 2005; **22**: 439-450 [PMID: 16163700 DOI: 10.1002/jmri.20404]
  - 64 **Hammond KE**, Lupo JM, Xu D, Metcalf M, Kelley DA, Pelletier D, Chang SM, Mukherjee P, Vigneron DB, Nelson SJ. Development of a robust method for generating 7.0 T multichannel phase images of the brain with application to normal volunteers and patients with neurological diseases. *Neuroimage* 2008; **39**: 1682-1692 [PMID: 18096412 DOI: 10.1016/j.neuroimage.2007.10.037]
  - 65 **Sehgal V**, Delproposto Z, Haddar D, Haacke EM, Sloan AE, Zamorano LJ, Barger G, Hu J, Xu Y, Prabhakaran KP, Elangovan IR, Neelavalli J, Reichenbach JR. Susceptibility-weighted imaging to visualize blood products and improve tumor contrast in the study of brain masses. *J Magn Reson Imaging* 2006; **24**: 41-51 [PMID: 16755540 DOI: 10.1002/jmri.20598]
  - 66 **Wu Z**, Mittal S, Kish K, Yu Y, Hu J, Haacke EM. Identification of calcification with MRI using susceptibility-weighted imaging: a case study. *J Magn Reson Imaging* 2009; **29**: 177-182 [PMID: 19097156 DOI: 10.1002/jmri.21617]
  - 67 **Zulfikar M**, Dumrongpisutikul N, Intrapiromkul J, Yousem DM. Detection of intratumoral calcification in oligodendrogliomas by susceptibility-weighted MR imaging. *AJNR Am J Neuroradiol* 2012; **33**: 858-864 [PMID: 22268093 DOI: 10.3174/ajnr.A2862]
  - 68 **Thamburaj K**, Radhakrishnan VV, Thomas B, Nair S, Menon G. Intratumoral microhemorrhages on T2\*-weighted gradient-echo imaging helps differentiate vestibular schwannoma from meningioma. *AJNR Am J Neuroradiol* 2008; **29**: 552-557 [PMID: 18079187 DOI: 10.3174/ajnr.A0887]
  - 69 **Toh CH**, Wei KC, Chang CN, Hsu PW, Wong HF, Ng SH, Castillo M, Lin CP. Differentiation of pyogenic brain abscesses from necrotic glioblastomas with use of susceptibility-weighted imaging. *AJNR Am J Neuroradiol* 2012; **33**: 1534-1538 [PMID: 22422181 DOI: 10.3174/ajnr.A2986]
  - 70 **Reichenbach JR**, Schweser F, Serres B, Deistung A. Quantitative Susceptibility Mapping: Concepts and Applications. *Clin Neuroradiol* 2015; **25** Suppl 2: 225-230 [PMID: 26198880 DOI: 10.1007/s00062-015-0432-9]
  - 71 **Eskreis-Winkler S**, Zhang Y, Zhang J, Liu Z, Dimov A, Gupta A, Wang Y. The clinical utility of QSM: disease diagnosis, medical management, and surgical planning. *NMR Biomed* 2017; **30**: [PMID: 27906525 DOI: 10.1002/nbm.3668]
  - 72 **He N**, Ling H, Ding B, Huang J, Zhang Y, Zhang Z, Liu C, Chen K, Yan F. Region-specific disturbed iron distribution in early idiopathic Parkinson's disease measured by quantitative susceptibility mapping. *Hum Brain Mapp* 2015; **36**: 4407-4420 [PMID: 26249218 DOI: 10.1002/hbm.22928]
  - 73 **Acosta-Cabrero J**, Williams GB, Cardenas-Blanco A, Arnold RJ, Lupson V, Nestor PJ. In vivo quantitative susceptibility mapping (QSM) in Alzheimer's disease. *PLoS One* 2013; **8**: e81093 [PMID: 24278382 DOI: 10.1371/journal.pone.0081093]
  - 74 **Moon Y**, Han SH, Moon WJ. Patterns of Brain Iron Accumulation in Vascular Dementia and Alzheimer's Dementia Using Quantitative Susceptibility Mapping Imaging. *J Alzheimers Dis* 2016; **51**: 737-745 [PMID: 26890777 DOI: 10.3233/JAD-151037]
  - 75 **Domínguez JF**, Ng AC, Poudel G, Stout JC, Churchyard A, Chua P, Egan GF, Georgiou-Karistianis N. Iron accumulation in the basal ganglia in Huntington's disease: cross-sectional data from the IMAGE-HD study. *J Neurol Neurosurg Psychiatry* 2016; **87**: 545-549 [PMID: 25952334 DOI: 10.1136/jnnp-2014-310183]
  - 76 **Walsh AJ**, Blevins G, Lebel RM, Seres P, Emery DJ, Wilman AH. Longitudinal MR imaging of iron in multiple sclerosis: an imaging marker of disease. *Radiology* 2014; **270**: 186-196 [PMID: 23925273 DOI: 10.1148/radiol.13130474]

**P- Reviewer:** Sergi CM, Schoenhagen P, Ueda H **S- Editor:** Ji FF  
**L- Editor:** A **E- Editor:** Tan WW





Published by **Baishideng Publishing Group Inc**  
7901 Stoneridge Drive, Suite 501, Pleasanton, CA 94588, USA  
Telephone: +1-925-223-8242  
Fax: +1-925-223-8243  
E-mail: [bpgoffice@wjgnet.com](mailto:bpgoffice@wjgnet.com)  
Help Desk: <http://www.f6publishing.com/helpdesk>  
<http://www.wjgnet.com>

